Desalination and Water Treatment
www.deswater.com
doi: 10.5004/dwt.2022.28096

248 (2022) 79–93
February

Wastewater treatment containing organic solvent from the production of hybrid membranes

Bruna Aline Araújo[a,*], Edcleide Maria Araújo[a], Karyna Steffane da Silva[b], Geralda Gilvânia Cavalcante de Lima[b], Keila Machado de Medeiros[c], Carlos Antônio Pereira de Lima[b]

[a]*Materials Engineering Department, Federal University of Campina Grande, Avenue Aprígio Veloso, 882, Bodocongó, 58429-900, Campina Grande, Paraiba, Brazil, emails: brunaaaraujo15@gmail.com (B.A. Araújo), edcleide.araujo@ufcg.edu.br (E.M. Araújo)*
[b]*Sanitary and Environmental Engineering Department, State University of Paraiba, Avenue Baraúnas, 351, Bodocongó, 58429-500, Campina Grande, Paraíba, Brazil, emails: karynasteffane@hotmail.com (K.S. da Silva), gilvania@uepb.edu.br (G.G.C. de Lima), caplima@uepb.edu.br (C.A.P. de Lima)*
[c]*Science and Technology Center in Energy and Sustainability, Federal University of Recôncavo da Bahia, Street Godofredo Rebello de Figueiredo Filho, 697, Sim, 44085-132, Feira de Santana, Bahia, Brazil, email: keilamedeiros@ufrb.edu.br (K.M. de Medeiros)*

Received 1 September 2021; Accepted 24 December 2021

ABSTRACT

In this work, titanium dioxide/ultraviolet (TiO_2/UV) heterogeneous photocatalysis was evaluated in degradation of N-methyl-2-pyrrolidone (NMP) because it is an organic solvent that has high chemical stability, treated by conventional processes. The effluents with NMP were obtained from the immersion bath and precipitation generated in obtaining the hybrid membranes by phase inversion technique. TiO_2 was characterized by X-ray fluorescence, X-ray diffraction, Fourier-transform infrared spectroscopy, particle size distribution, textural analysis, differential scanning calorimetry and thermogravimetry. The effluent was evaluated by hydrogen potential, electrical conductivity, turbidity, and chemical oxygen demand. The semiconductor presented 98.6% a purity grade, predominant crystalline phase anatase, TiO_2 characteristic bands, average particle diameter of 59.6 nm and endothermic peaks up to 100°C, which are considered important intrinsic characteristics for application in photocatalytic processes. Kinetic assays were performed following the experimental design and the kinetic data were fitted to the pseudo-first-order model. For photocatalytic degradation response, all variables showed a significant effect at the 95% confidence interval. The Statistical tool detected that pH had the greatest influence and its ratio was directly proportional to the degradation of contaminants. Therefore, it was found that the TiO_2/UV process showed photodegradation potential of 95% of the organic solvent NMP.

Keywords: Photocatalysis; Titanium dioxide; N-methyl-2-pyrrolidone; Contaminated water

1. Introduction

Environmental impacts are becoming increasingly critical and frequent, and natural waters have been identified as one of the most degraded type of water resource. In this sense, water quality control standards and regulations against hazardous pollutants have become more stringent in many countries. These effluents when not treated correctly, in addition to being a source of visual pollution, present several risks of environmental impact, mainly

* Corresponding author.

due to interference with natural photosynthetic processes, causing incalculable damage to the entire aquatic biota.

The inappropriate disposal of these organic effluents has generated concern for the scientific community, which has the challenge of applying more efficient repair processes for this kind environmental damage [1].

Discussions about the environment are becoming more and more important and appearing more frequently all over the world, along with the topic of natural waters that has been pointed out as one of the most degraded natural resource by the world's population. As a result, the current quality control bodies are becoming more and more stringent against the various existing pollutants. Such effluents, when not treated correctly, besides being a source of pollution, can considerably increase environmental impacts, and thus, cause practically permanent damage to all existing aquatic biota. The impact that these effluents can have on the environment and for the population is of great concern to authorities, because they have great carcinogenic potential [2].

Many of the effluents generated in laboratories are colored organic liquid wastes and by-products of chemical reactions that are difficult to treat. They are directly disposed in laboratory sinks, causing negative environmental impacts [3]. Effluents containing organic compounds with different functionalities are difficult to treat by classical methods, such as coagulation, flotation, sedimentation, and adsorption. Furthermore, all these treatments mentioned above are not effective, as they simply transfer the pollutants from one phase to another, instead of destroying them, which consequently leads to secondary pollution [4]. However, searches to improve the adsorption efficiency are continuously pursued through new adsorbents with special characters, while the removal process is carried out under optimal operating conditions [5].

The concern with wastewater treatment is not restricted to the industrial field. A new concept of sustainable chemistry has recently emerged, which advocates the degradation of waste, whether in industrial or laboratory effluents. The concept of sustainable chemistry is the creation, development and application of chemical products and processes to eliminate the generation of toxic substances [6]. This requires specific studies for process improvement, using various catalytic and photocatalytic materials with the fundamental goal of treating toxic waste and effluents [7–17].

The numerous discoveries in nanoscience, nanotechnology, and recent innovations in the field of catalytic treatment of gaseous effluents, water, sewage and soil, mean that heterogeneous photocatalysis combined with other treatment techniques are always evolving in the environmental area [18]. For this, there is a great need to develop new ways to reduce the environmental impacts generated from obtaining membranes. Studies have been conducted on advanced oxidative processes (AOPs) such as photocatalysis with titanium dioxide/ultraviolet radiation (TiO_2/UV), where they present greater efficiency in the treatment of these effluents. The AOP's are based on the use of highly oxidizing species to promote a more effective degradation of the pollutant and can be used in combination with biological treatments to increase the biodegradability of recalcitrant compounds [19,20].

Heterogeneous photocatalysis is a process in which a semiconductor absorbs photon energy and acts as a catalyst producing reactive radicals, especially hydroxyl radicals, which can oxidize and mineralize organic compounds. Therefore, these organic molecules are decomposed to form carbon dioxide, water, and mineral acids [18]. TiO_2 is the most used semiconductor in photocatalysis and many catalysts containing TiO_2 have been developed to improve $^{\bullet}OH$ production, reduce the band gap energy, delay e^-/h^+ recombination, increase its reaction area and affinity for organic compounds and reduce the cost catalyst recovery after use [21].

TiO_2 nanoparticles are excited by UV light in water, generating $^{\bullet}OH$ in contact with dissolved oxygen. Oxygen is required for an efficient photocatalysis process [22].

To understand the mechanism of this process, the nanoparticles are illuminated by light/UV, so that the electrons of the nanoparticles tend to stay in the conduction band. This process generates a gap in the valence band, in which the generation of highly oxidizing properties originates. In fact, the presence of electrons in the conduction band and a gap in the valence band are responsible for the highly oxidizing characteristics of these TiO_2 nanoparticles [23]. Therefore, the use of TiO_2 offers an advantage over photolysis processes by accelerating the destruction of unwanted organic matter [24]. The reaction of TiO_2 in the presence of UV radiation is described [25] by Eqs. (1)–(10).

Photoactivation of the semiconductor particle:

$$TiO_2 + h\nu \rightarrow h^+_{BV} + e^-_{BC} \quad (1)$$

Reaction between the photogenerated gap and the adsorbed water:

$$h^+_{BV} + H_2O \rightarrow {}^{\bullet}OH + H^+ \quad (2)$$

Reaction between the photogenerated gap and the OH^- groups on the surface of the TiO_2 particle:

$$h^+_{BV} + OH^- \rightarrow {}^{\bullet}OH \quad (3)$$

Superoxide radical ion formation:

$$O_2 + e^-_{BC}\ h\nu \rightarrow h^+_{BV} + O_2^{\bullet -} \quad (4)$$

Hydrogen peroxide formation:

$$O_2^{\bullet -} + H^+ \rightarrow HO_2^{\bullet} \quad (5)$$

$$HO_2^{\bullet} + HO_2^{\bullet} \rightarrow H_2O_2 + O_2 \quad (6)$$

$$O_2^{\bullet -} + HO_2^{\bullet} \rightarrow HO_2^- + O_2 \quad (7)$$

$$HO_2^- + H^+ \rightarrow H_2O_2 \quad (8)$$

Generation of hydroxyl radicals by breakdown of hydrogen peroxide:

$$H_2O_2 + e^-_{BC} \rightarrow {}^{\bullet}OH + OH^- \quad (9)$$

Breakdown of the hydrogen peroxide molecule under irradiation (photolysis) with the production of hydroxyl radicals:

$$H_2O_2 + h\nu \rightarrow 2^{\bullet}OH \quad (10)$$

The reaction between the substrate and the hydroxyl radicals on the catalyst surface can occur in several ways. The hydroxyl radical can attack an adjacent adsorbed molecule, it can attack a molecule in solution, it can diffuse across the surface and subsequently react with the adsorbate or molecule in solution; and it can free itself from the semiconductor surface and migrate into solution as a free radical. Most studies on heterogeneous photocatalysis with TiO_2 indicates that the attack of the hydroxyl radical on the substrate is the first step in the oxidative mechanism. The mechanism of photocatalytic oxidation of organic compounds will be via radicals in solution or directly on the catalyst surface, depending on the substrate and the reaction conditions. In most cases what occurs is the integration of the two mechanisms, with one of them prevailing over the other [26].

Membranes fabrication uses toxic organic solvents, such as N-methyl-2-pyrrolidone (NMP), formic acid (FA) and N,N-dimethylformamide (DMF) by the phase inversion technique, which is the most widely used to obtain polymeric and hybrid microporous membranes and are produced by precipitation of the solution in a non-solvent bath, generating effluent [27].

These solvents mix with water during the formation of the polymeric membrane and, consequently, generates significant amounts of effluent or wastewater containing such solvents. Due to the polluting nature of membrane manufacturing, it has been observed that the downstream process path of membrane technology only becomes more sustainable when the distilled amount is greater than 100 L m^{-2} of solvent processed [28].

In the manufacturing process of polymeric membranes, the solvent NMP is widely used, being in high concentration above 1,000 mg L^{-1}. Its disposal is of great concern, requiring treatment, due to possible negative environmental impacts. Loh et al. [29] studied a way to treat wastewater from the membrane manufacturing process containing higher concentration of NMP by a sequential batch reactor (SBR) and by a membrane bioreactor (MBR). The authors concluded that the SBR treatment was able to remove more than 90% of the dissolved organic carbon and approximately 98% of the NMP within 2 h of the experiment. However, the MBR experiment showed a decrease in efficiency from 100% to 40% within 15 d of operation.

Despite the great interest of the entire academic and business community in the production of polymeric membranes, where numerous works are being developed and published, it is observed that almost none address the problem of effluents generated in the processes for obtaining this product. The process of obtaining these membranes by the phase inversion immersion-precipitation method produces a considerable volume of effluents that are inadequate to be directly disposed of into the receiving water bodies. Thus, a need for studies on the treatment of these effluents arises, both for disposal and for the possibility of reusing the treated effluent in the process itself. The treatment of effluents generated in membrane production processes is necessary, because it is highly damaging to the environment due to the high chemical oxygen demand (COD), and the presence of several chemical compounds such as organic acids [30].

Therefore, the effluent generated from membrane production has a high organic load, composed of synthetic non-biodegradable substances, such as NMP, FA and DMF, where treatment by conventional methods (coagulation, flotation, sedimentation, and adsorption) is not sufficient to treat the recalcitrant substances present in them.

Membrane manufacturing produces a very large volume of contaminated water as a result of the solvent and non-solvent immersion and precipitation method. This generated effluent needs to undergo appropriate, efficient, fast, and economically feasible treatments. Given the above, the objective of this work is the application of TiO_2/UV photocatalysis in degradation of the solvent NMP contained in effluents generated in production of membranes, which are extremely aggressive substances to the environment.

2. Experimental

2.1. Materials

For this research, the following materials were used: titanium dioxide (TiO_2) was P-25, identified as Aeroxide® with a purity grade of 99.5% in fine powder form, Fig. 1, supplied by Evonik Industries Degussa, which consists of 70% of anatase phase and 30% of rutile phase and the solvent N-methyl-2-pyrrolidone (NMP) P.A./ACS, C_5H_9NO, with purity of 99.5%, from the company Labsynth.

2.2. Preparation of membranes

The membranes were prepared by the immersion-precipitation method, which is the most widely used in the phase inversion technique. This process consists of depositing a polysulfone solution on a glass plate, forming a thin film that was exposed for a certain time and then immersed in a non-solvent bath (water) to the formation of the membrane. In this process, an effluent is generated containing the NMP, which was treated with TiO_2/UV heterogeneous photocatalysis, obtaining the complete mineralization of the NMP with the production of CO_2 and water, as shown in Fig. 2.

Fig. 1. Chemical structure: (a) titanium dioxide and (b) N-methyl-2-pyrrolidone.

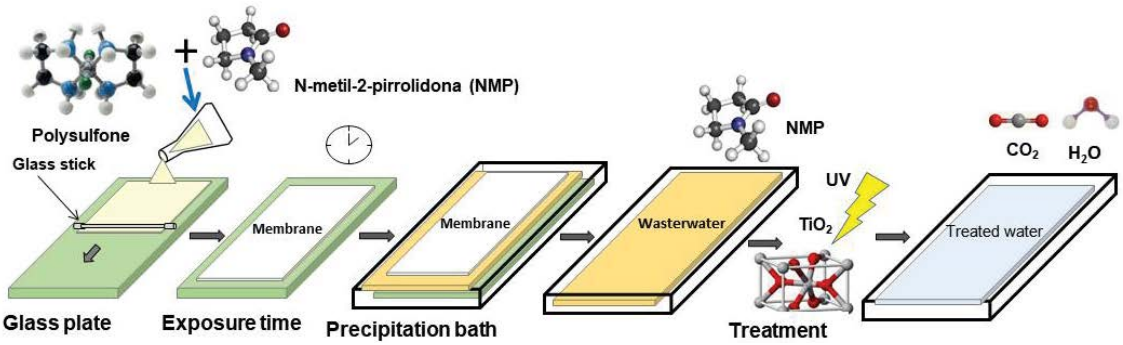

Fig. 2. Treatment by heterogeneous photocatalysis of the effluent containing NMP generated in preparation polymeric membranes by the phase inversion technique.

2.3. Collection of effluents generated in the production of the membranes

Synthetic effluents were prepared to simulate the real effluent. These contain recalcitrant compounds containing NMP at concentrations of 1.01 and 5.04 μM, which are aggressive substances, that cause damage to the environment if there is no type of treatment before disposal. In each experiment, 1000 mL of effluent was used, where variable amounts of photocatalyst (TiO_2) were introduced (0.1% and 0.3%). Before starting the experiments, the pH of the effluent was adjusted to 5 using 0.1 M hydrochloric acid (HCl) and to 9 using 0.1 M sodium hydroxide (NaOH).

2.4. Photocatalyst characterizations

The Chemical analysis was performed using X-ray fluorescence in an X-ray energy dispersive spectroscopy apparatus in the Shimadzu EDX 700 instrument. The X-ray diffraction (XRD) was performed on Shimadzu XDR-6000 equipment, using Cu kα radiation (λ = 1.5418 Å), 40 kV voltage, 30 mA current, 2°–75° scan and a scan rate of 2° min^{-1}. Fourier-transform infrared spectroscopy (FTIR) was performed on a Perkin Elmer model 400 FTIR/FT-NIR spectrometer, between 4,000 and 400 cm^{-1}, with a resolution of 4 cm^{-1} and 20 scans. The particle size distribution was performed on a Mastersizer 2,000 instrument. Textural characteristics were determined using the N_2 adsorption/desorption technique in Quantachrome equipment, model Nova 3200.

For the differential scanning calorimetry (DSC) about 5 mg of the sample was used, heated at a rate of 10°C/min^{-1} in nitrogen atmosphere and temperature range of 20°C–360°C. Thermogravimetric analysis (TG) was performed in a thermal analyzer, model RB-3000-20, with a heating rate of 10°C/min^{-1}, in nitrogen atmosphere, using an alumina crucible and an ambient temperature range (25°C) up to a maximum temperature of 1,000°C, and with 5 mg of sample. All characterizations were performed out in the laboratories of the Materials Engineering Academic Unit of the Federal University of Campina Grande, Campina Grande-PB, Brazil.

2.5. Parameters for effluent analysis

The pH parameter is important and has a great influence on photocatalytic processes. Variations in pH value cause changes in the semiconductor/liquid interface, leading to changes in the redox potentials and adsorption, and desorption properties of the catalyst. In some cases, pH is the main factor influencing the degradation rate of the substrate subjected to the photocatalytic process. Conductivity is the measurement resulting from the application of a given electrical force, which is directly proportional to the number of salts present in a solution. This parameter does not specifically determine which ions are present in each water sample, but it can contribute to possible recognition of environmental impacts that occur in the drainage basin by discharges of industrial or domestic waste.

Measurement of turbidity was carried out using a nephelometer. This method is based on comparing the intensity of light deflected by the sample, with the intensity of light deflected by a standard reference suspension. The magnitude of turbidity is directly related to the intensity of the stray light. A standard 40 NTU mold suspension has an approximate turbidity of 40 NTU, so nephelometric turbidity units based on a mold standard will approximate the turbidity units obtained in a Jackson turbidimeter but will not be the same. Determination of COD consisted of the procedure based on the oxidation of organic matter using the remaining potassium dichromate ($K_2Cr_2O_7$) as an oxidant. The reaction occurred in the presence of sulfuric acid (H_2SO_4), with the action of silver ions as a catalyst. The aqueous solution was heated at closed reflux for 120 min at 150°C.

The physicochemical parameters (Table 1) pH, electrical conductivity and turbidity were analyzed. The methodologies used to obtain all the physicochemical parameters of the water from the precipitation bath generated in production of membranes are recommended in Standard Methods for Examination of Water and Wastewater [31]. The analyzes were carried out in laboratory of Department of Sanitary and Environmental Engineering of the Paraíba State University, Campina Grande-PB, Brazil.

2.6. Photocatalytic process

The photocatalytic oxidation studies for solvent degradation were carried out in a glass reactor with a capacity of 1,000 mL, and room temperature during the tests was kept. Magnetic stirring kept the TiO_2 in suspension. Fig. 3a and b.

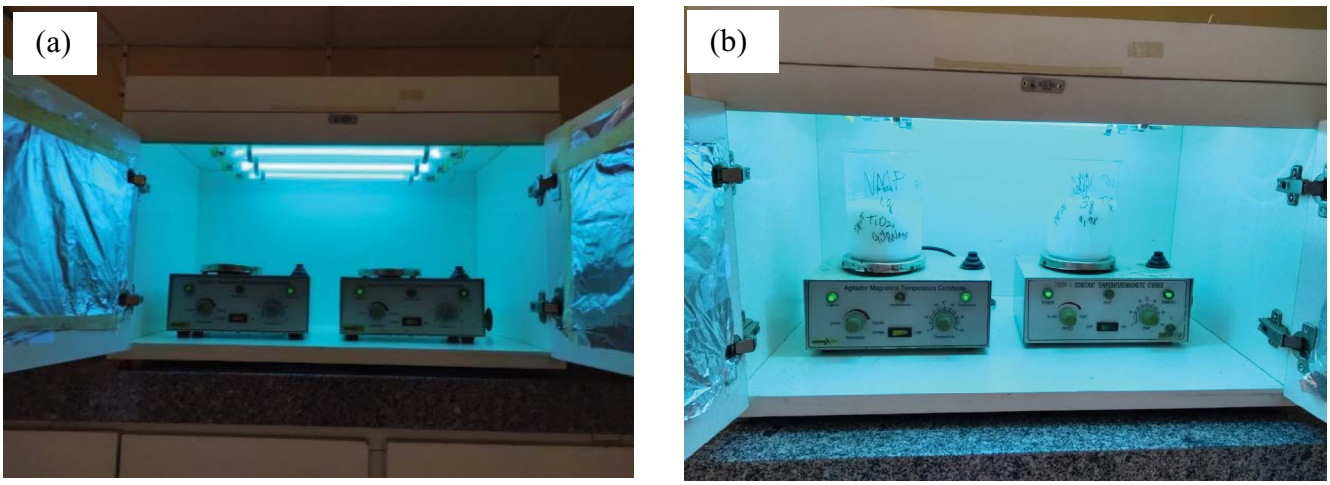

Fig. 3. (a) System camera and (b) experimental system in synthetic effluent.

Table 1
Physical–chemical parameters analyzed and equipment used

Parameter	Equipment
pH	pH meter
Electrical conductivity, μS cm^{-1}	Conductivity meter
Turbidity, NTU	Nephelometric
COD, mg O_2 L^{-1}	Closed reflux

Ultraviolet radiation was provided by three germicidal lamps, 15 W each, the volume used was 1,000 mL, and the pH values and the amount of TiO_2 photocatalyst were optimized for photocatalysis. The pH of the effluents was adjusted using HCl or NaOH. All experiments were performed three times. The photocatalytic activity of a semiconductor occurs as a result of the production of excited electrons under UV irradiation in its conduction band, along with corresponding positive gaps in the valence band, which reacts with contaminants adsorbed on the photocatalyst surface. Photocatalyst concentration used cannot be too high, as excessive amounts hinder the passage of light in the working solution, reducing the efficiency of the system [32].

In photocatalysis, as UV light activates TiO_2, holes and electrons are generated in the valence band (VB) and conduction band (CB). Since most semiconductors are composed of nanocrystalline solids, the charges on the electrons/holes can migrate to the surface of the particle, reducing the oxygen molecule when superoxide radicals are formed. Holes in VB oxidize hydroxyl groups and water to form hydroxyl and peroxide radicals. The radicals break down organic molecules into non-toxic products [33].

2.7. Kinetic analysis

The experimental data of photocatalytic degradation of the NMP solvent were fitted to the Langmuir-Hinshelwood (L-H) model proposed by Eq. (11):

$$r = -\frac{dC}{dt} = \frac{k_r \cdot k_a \cdot C}{1 + k_a \cdot C} \tag{11}$$

where r (μmol L^{-1} min^{-1}), k_r (μmol L^{-1} min^{-1}), k_a (L μmol^{-1}), C (μmol L^{-1}) and t (min) are the reaction rate, reaction rate constant, adsorption constant, reagent concentration and irradiation time, respectively [34–37]. With low initial solvent concentration, the rate expression (Eq. (11)) can be demonstrated in the form of Eq. (12):

$$r = -\frac{dC}{dt} = k_r \cdot k_a \cdot C = k \cdot C \tag{12}$$

where k is the pseudo-first-order rate constant and by integrating Eq. (12) with the limit of $C = C_0$ at $t = 0$, results to Eq. (13):

$$\ln\left(\frac{C}{C_0}\right) = -k \cdot t \tag{13}$$

where C_0 is the amount of initial organic matter, C is the is the sum degradations at each time of the solvent solution and surface. According to Eq. (13), the plot of $\ln(C/C_0)$ vs. t for all degradations should be linear, with the values of k being obtained directly from its slope. One of the most useful indications for evaluating the reaction rate of first-order kinetics is the calculation of the half-life time of the reaction. The half-life ($t_{1/2}$) was calculated by Eq. (14) as follows:

$$t_{1/2} = \frac{\ln(2)}{k} \tag{14}$$

2.8. Calculation of degradation efficiency

The degradation efficiency (η) of the solvents at a reaction time t (min) was calculated as follows in Eq. (15):

$$\eta = \frac{COD_0 - COD}{COD_0} \times 100\% \tag{15}$$

where COD_0 is the initial effluent organic matter concentration (mg O_2 L^{-1}); COD is the final effluent organic matter concentration (mg O_2 L^{-1}) at the reaction time t (min).

3. Results and discussion

3.1. Photocatalyst characterization

3.1.1. X-ray fluorescence

The chemical composition of the TiO_2 was determined through X-ray fluorescence data. Table 2 shows the chemical composition in % by weight, normalized to 100% oxides.

It was possible to prove that the TiO_2 presents a purity of 98.6%, with the presence of secondary mineral oxides, through the semi-quantitative technique [38]. The data obtained corroborate with the composition of Degussa P25 material as described in the manufacturer's file (TiO_2 min 98%). The detection of phosphorus pentoxide by XFR is predicted by the manufacturer (0%–2%) and could indicate the presence of some type of phosphate and potassium based additive as a dispersant due to its main application as a pigment. The presence of secondary oxides can accelerate or delay the transformation of anatase-rutile phase, due increase or decrease in the concentration of vacancies present in crystalline phases of the sample.

3.1.2. X-ray diffraction

By X-ray diffraction, it was possible to identify the phases and crystal planes in the sample, as can be seen in Fig. 4.

According to the diffractogram shown in Fig. 4, it can be seen that the crystalline characteristic phases of TiO_2 were anatase and rutile. The characteristic diffraction peaks of TiO_2 anatase phase are 2θ = 25.4°, 37.9°, 38.4°, 38.7°, 48.3°, 54.0°, 62.2°, 62.9°, 68.8°, 70.5° and of the crystalline planes (101), (103), (004), (112), (200), (105), (213), (204), (116) and (220), respectively. In addition, in the XRD pattern, the characteristic peaks rutile phase of TiO_2 were observed for to 2θ = 37.8°, 44.5°, 55.5°, 64.8° and crystalline planes (101), (210), (211) and (310), respectively.

Therefore, the samples prevailed in the anatase phase, confirming that the material used as a source of TiO_2 was Degussa P25, which consists of 70% anatase and 30% rutile [36,39]. The photocatalytic activity of TiO_2 is strongly dependent on its crystallite size, phase structure, porous structure and specific surface area. Due to a greater band gap (3.2 eV) of anatase than that of rutile (3.0 eV), anatase has lower absorbance capacity relative to sunlight [40].

The photocatalytic activity of anatase is apparently superior to rutile. This is due to the lower charge carrier recombination rate of this anatase and higher surface adsorption capacity to hydroxyl groups [41]. The anatase crystalline is the greater phase. This feature is important because it is the most photoactive phase of titanium dioxide, which is highly desirable in photocatalytic degradation processes [42,43].

X-rays have wavelength between 0.01–10 nm. Consequently, X-rays can easily penetrate inside the crystal structure of any material; and it tells the properties of the material, as it exits that material. Which is why X-ray spectroscopy is a very useful technique for characterization of ceramics materials. We can easily calculate the average crystallite size from Scherrer formula [44] given by Eq. (16):

Table 2
TiO_2 purity and amount of impurities semiquantified

Constituent	Percentage (%)
TiO_2	98.60
Sb_2O_3	0.46
P_2O_5	0.40
K_2O	0.36
SO_3	0.10
NbO	0.03
ZrO_2	0.02

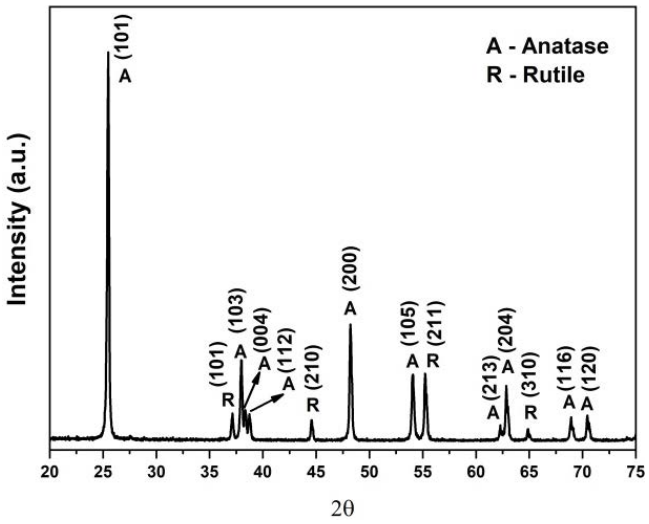

Fig. 4. XRD diffractogram of TiO_2.

$$D_p = \frac{0.94\lambda}{\beta \mathrm{Cos}\theta} \tag{16}$$

where D_p = average crystallite size, β = line broadening in radians, θ = Bragg angle, λ = X-ray wavelength.

Scherrer equation, in X-ray diffraction and crystallography, is a formula that relates the size of submicron crystallites in a solid to the broadening of a peak in a diffraction pattern. It is often used in determining the size of crystals in powder form. The crystallite size found was 42.56 nm and can be considered a lower limit of the TiO_2 particle size [45].

3.1.3. Fourier-transform infrared spectroscopy

The results of FTIR analysis of the characteristic bands of titanium dioxide can be seen in Fig. 5.

In Fig. 5 the FTIR spectrum band shows that the peak of absorbance at band 505 cm^{-1} is due to the vibration of Ti–O connection and the peak at 612 cm^{-1} is attributed to vibration of the Ti–O–O connection [46,47]. The range between 403–978 cm^{-1} was due to vibrations of six octahedra of

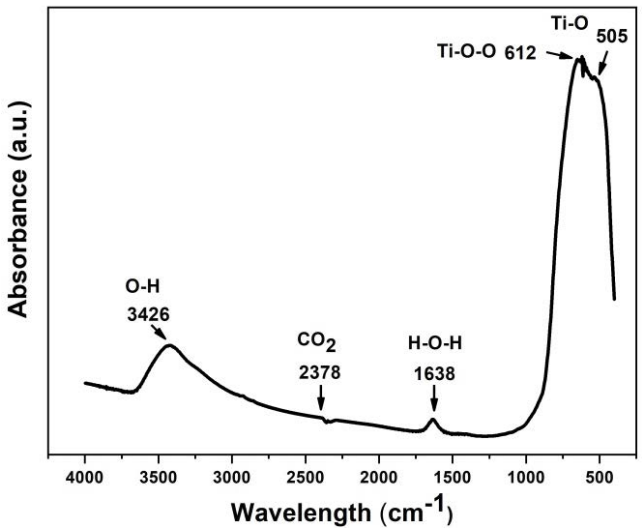

Fig. 5. TiO_2 FTIR spectrum.

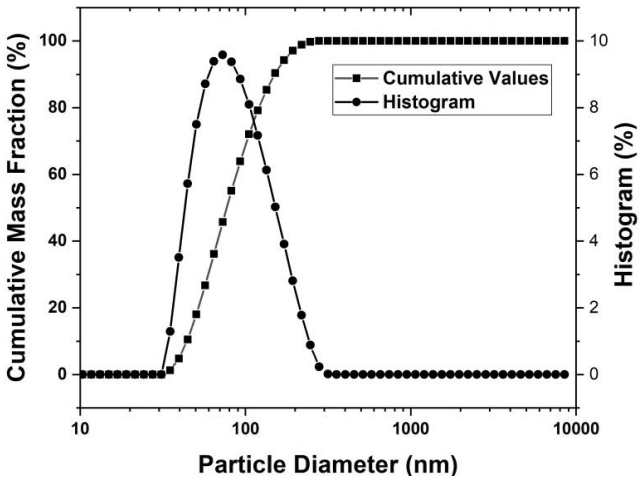

Fig. 6. TiO_2 granulometric distribution.

coordinated TiO_6 and four by coordinated Ti–O titania anatase. The bandwidth at 1,638 cm^{-1} is assigned to the H–O–H connection of the physisorbed water [48]. The bandwidth at 2,378 cm^{-1} is attributed to CO_2 present in the atmosphere [49]. For the TiO_2 sample, the spectrum presents a strong absorption bandwidth at 3,426 cm^{-1}, corresponding to the –OH isolate, related to the –OH stretch attributed to surface water adsorbed by the TiO_2 sample. The amount of O–H groups adsorbed on the catalyst surface is responsible for improving the photocatalytic efficiency [50].

3.1.4. Granulometric distribution (GD)

Fig. 6 illustrates the particle size distribution and the average diameter of TiO_2 particles. Knowledge of the statistical granulometric distribution and elemental particle size is essential, as it significantly influences the microstructure, affecting the density, thermal, electrical, and photocatalytic properties of semiconductor. Therefore, determining the particle size of TiO_2 and proving its nanoparticles through particle size distribution is extremely important to act more efficiently in the photocatalytic process.

In Fig. 6 it can be seen that the frequency histogram curve for the TiO_2 particle size distribution is unimodal an average particle diameter of 59.6 nm. The size distribution range extends from 30 to 300 nm [51,52]. About 57.35% of the accumulated particles are smaller than 87.8 nm. The narrower the distribution shown by the particle diameter curve, the greater the homogeneity with respect to the particle distribution, size and geometry.

Also, according to Fig. 6, the d_{10} = 10% of the obtained particles had diameters smaller than 46.1 nm, d_{50} = 50% of the particles had diameters smaller than 76.8 nm and d_{90} = 90% of the particles had diameters smaller than 158.6 nm [53]. Furthermore, the decrease in particle size is accompanied by an increase in the surface/volume ratio, which makes the surface energy contribute significantly to the total energy of material. This means that for small particles, the polymorphic form with the lowest surface energy has the highest thermodynamic stability, which contributes to a better performance of the photocatalytic process [54].

3.1.5. Differential scanning calorimetry

Differential scanning calorimetry is a technique used to determine the heat flux in and out of a sample when subjected to a temperature program in a controlled atmosphere. From DSC curve, when heating a sample, thermal changes in a material are accompanied by a heat exchange, so the temperature of these transformations and heat flux can be determined. Fig. 7 illustrates the DSC curve.

In Fig. 7 two endothermic events can be observed: at 54°C, which can be related to physisorption of water on the surface; and at 218°C, which can be attributed to water leaving the constitution and formation of TiO_2 [55]. It is important to note that a wider temperature range up to 1,000°C could reveal other events, which would make it possible to assign the transition temperatures from amorphous to anatase assign and from anatase to rutile. However, the DSC analysis instrument used did not allow obtaining events above 350°C, and it was necessary to perform a TG to increase the temperature range and be able to observe the phase transitions that occurred in TiO_2.

3.1.6. Thermogravimetric analysis

TG follows the mass changes in a sample that has undergone heat treatment. The TG analysis can be recorded as a change in sample mass with temperature and time, and with gas pressure and composition. Fig. 8 illustrates TG curves and the thermogravimetric analysis derivative (DTG). From the TG curve and its derivative, a total mass loss of 4% was evidenced for TiO_2 and the detected mass loss events occurred in four stages of decomposition: at 41°C referring to water desorption, at 262°C inherent in the loss of crystalline TiO_2 water, eliminating the hydroxyl group as water vapor by condensation of Ti–OH groups, producing the Ti–O–Ti bond; at 483°C related to the conversion of $Ti(OH)_4$ into TiO_2, indicating the beginning of the

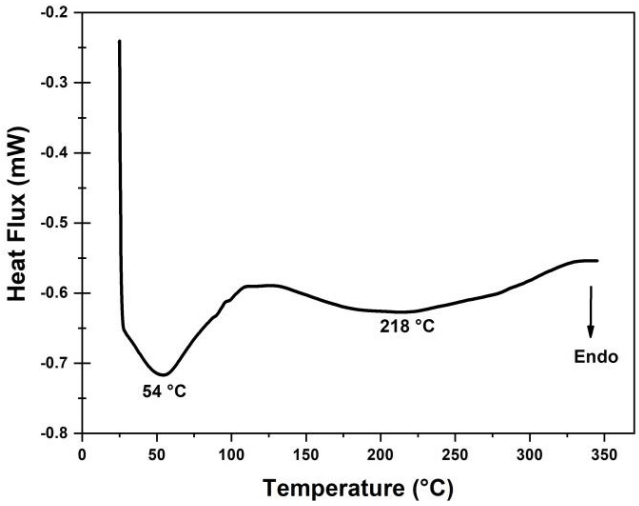

Fig. 7. TiO_2 DSC curves.

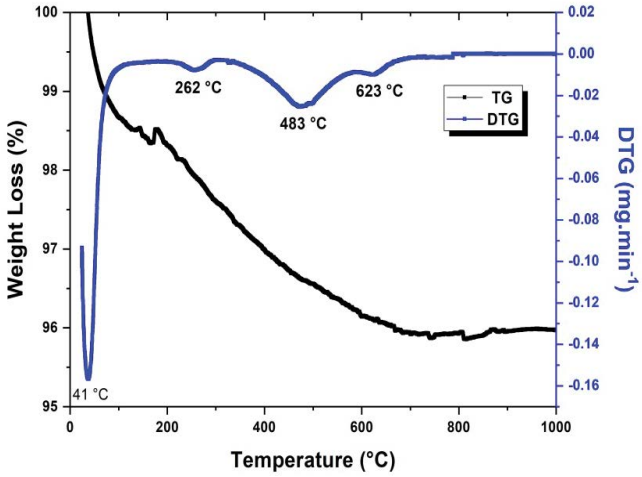

Fig. 8. TiO_2 TG and DTG curves.

structural organization of the system, which will possibly induce crystallization of the amorphous phase by the anatase; and at 623°C probably corresponds to the transition from the anatase phase to rutile phase [56–58].

According to DSC and TG/DTG in Figs. 7 and 8 it was found that the endothermic peaks between room temperature to 100°C came from free water and water molecules physically adsorbed on the TiO_2 surface by hydrogen bonds, since both molecular and dissociated water (–OH groups) adsorbed on the semiconductor favors the photocatalytic process [59,60].

3.2. Photocatalytic process

3.2.1. Chemical oxygen demand

One of the most important parameters influencing the photocatalytic degradation of solvents is the pH, due to its effect on the properties related to the photocatalyst surface and influences on the ionic species in the solution.

The pH of treated solution is one of the variables with the greatest influence on the photocatalytic degradation of pollutants, because it affects several physicochemical properties of the photocatalyst, which tends to increase or reduce the degradation efficiency [32]. Therefore, the effects of pH were investigated on the photocatalytic activity of the effluent containing the solvent NMP.

The pH value in the COD photocatalytic process plays an important role during the degradation of the NMP contaminant, as illustrated in Fig. 9a and b. Through pH, it is possible to identify the intrinsic characteristic of the photocatalyst, which allows determining whether the surface of the solution is negatively or positively charged [61].

The COD experiments were performed with pH values set before analysis at pH 5 and pH 9, as shown in Fig. 9a and b. The solvent concentrations were varied at 1.01 and 5.04 μM NMP with photocatalyst loadings at 0.1% and 0.3%, following the experimental design. In the analysis for the NMP solvent, before starting the system, the adsorption and desorption balance between the photocatalyst loading and

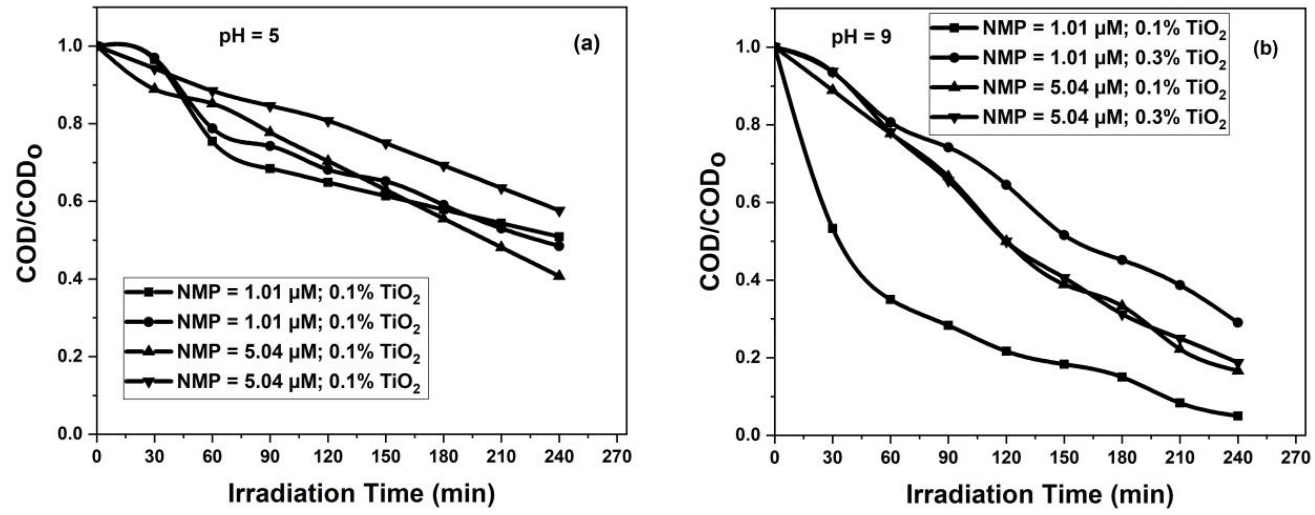

Fig. 9. Efficiency curve of NMP photocatalytic process (a) pH 5 and (b) pH 9.

the solvent was confirmed. Then, the effluent was exposed to irradiation for 240 min to ensure the photocatalytic process (TiO_2/UV). Therefore, it was possible to observe that the higher the pH, the greater the degradation of the solvent. The degradation that presented the best performance reached 95%. For the pH set at 5, the maximum degradation reached 59%. Changing the pH alters the charge on the surface of TiO_2 particles, changing the potential of the catalyst reactions. The solvent degradation efficiency was most effective at low concentrations of catalyst loading with the lowest concentration of solvent NMP. This fact was most evident at pH 9.

3.2.2. Potential of hydrogen (pH)

One of the most important parameters influencing the photocatalytic degradation of a pollutant is the pH. This is due to the effect of pH on the charging properties of the surface of the photocatalyst surface and the influences on the ionic species in the solution [62].

The pH analysis for all experiments with the NMP solvent can be seen in Fig. 10a and b. Fig. 10a illustrates the pH set at 5, where the effect of the initial concentration of the NMP solvent along with the catalyst loading was not as significant as compared to pH 9, Fig. 10b. In this case, more concentrated solutions will absorb UV radiation, competing with the photocatalyst (TiO_2) and, consequently, fewer photons will absorb the photocatalyst to generate hydroxyl radicals to promote the reactions [63]. Fig. 10b shows a pH of 9, where it can be seen that from the beginning of the process, a considerable decrease in the time interval of 30 min. This fact shows that the effect of pH is quite relevant for the degradation rates. Therefore, in general, it was observed that the higher the pH, the higher the degradation rate.

The pH variation changes the charge on the surface of the TiO_2 particles and varies the potential of the catalyst reactions.

With the variation of potential, the adsorption of the contaminant on the catalyst surface varies and, as a result, causes variation in the reaction speed. Under acidic and alkaline surface conditions, TiO_2 can be a pseudo proton and/or obtain negative charge, respectively.

Since NMP is an aprotic dipolar solvent and the surface of TiO_2 particles in alkaline medium has a negative charge and cationic types can be easily adsorbed, photodegradation is done better under basic conditions [64]. This fact shows that the effect of pH is quite relevant to the degradation rates. Therefore, in general, it was observed that the higher the pH, the higher the degradation rate.

3.2.3. Turbidity

Turbidity for the solvent NMP is illustrated in Fig. 11a and b. At time 0, the turbidity is low for all experiments as there is no TiO_2. The turbidity increases when TiO_2 is added, reaching 866 UNT in Fig. 11a due to the high photocatalyst loading and the high solvent concentration in 30 min. For pH 9, Fig. 11b, the turbidity reaches its higher level of about 21 UNT, but subsequently, there is a decrease of it, almost equaling the turbidity at the beginning of the process.

For effluents containing a higher catalyst loading, a lower pH and a higher solvent concentration, turbidity values are quite high, but after treatment they decrease. At higher pH, lower solvent concentration, and lower catalyst loading, the turbidity indices were lower, approaching the initial time value. For NMP, the largest decrease in turbidity occurred at a lower catalyst loading concentration, a lower amount of solvent concentration and a higher pH value. The increase that occurs in the interval from 0 to 30 min occurred because the raw effluent contains no catalyst loading, with the presence of loading its turbidity increases, and after the treatment the turbidity shows a good decay over 240 min.

For the effluents containing higher catalyst loading, lower pH and higher solvent concentration, the highest turbidity values were obtained, but after the treatment for more than 240 min, there was a significant decrease in turbidity.

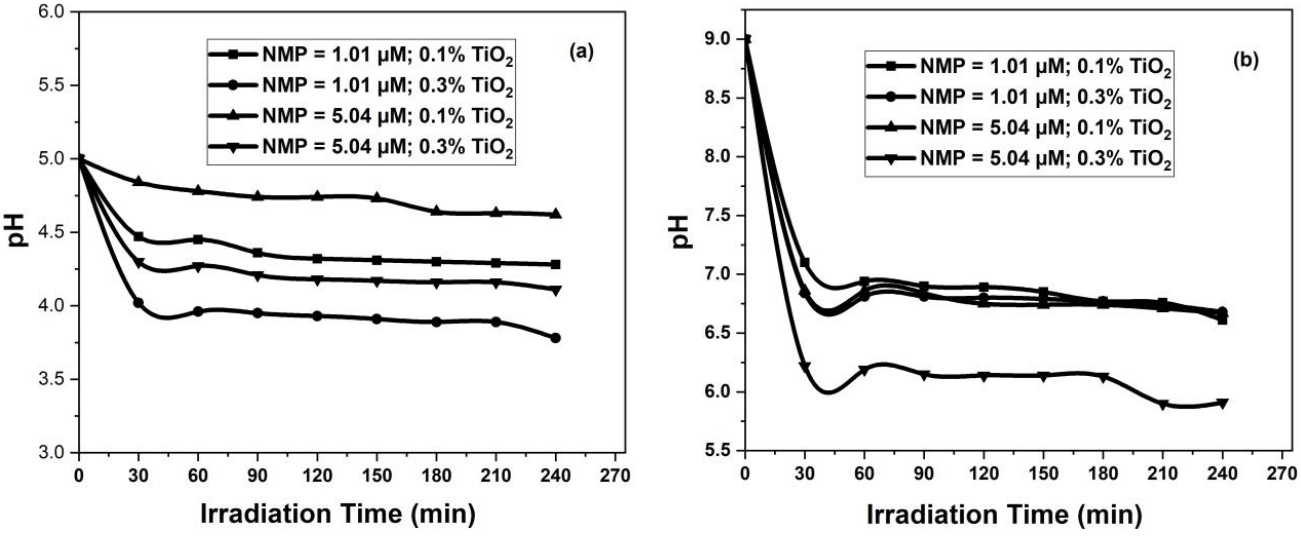

Fig. 10. pH curve for NMP (a) pH 5 and (b) pH 9.

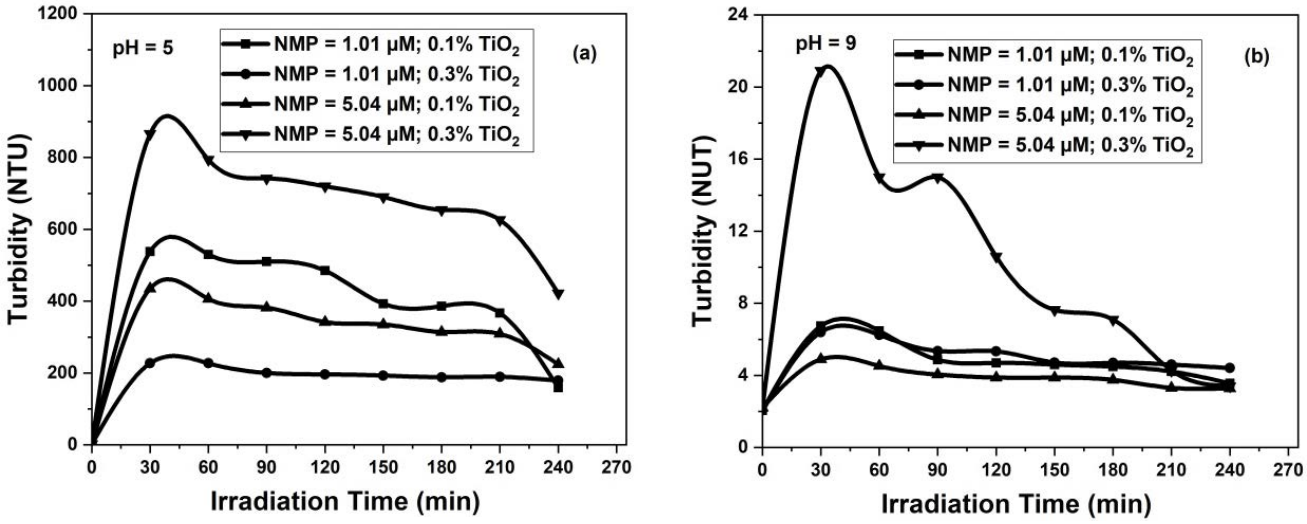

Fig. 11. Turbidity curve for NMP (a) pH 5 and (b) pH 9.

3.2.4. Electric conductivity (EC)

Fig. 12a and b show the electrical conductivity analysis for the NMP solvent. Electrical conductivity is related to the ionic content present in a solution and indicates the ability of water to transmit electrical current due to the presence of dissolved substances that dissociate into anions and cations and is therefore directly proportional to the ionic concentration. In general, it was found that the conductivities of the effluents increased due to mineralization. In addition, it was possible to identify that, because the solvent was of organic nature, independent of the pH studied, the conductivity was slightly low [65].

The kinetic study was prepared from the results obtained in experimental planning, where the response variable of the experimental data was used. The photocatalytic activities of NMP solvent were measured using degradation kinetics. It is known that the photocatalytic activity of TiO_2 is strongly influenced by the crystalline phase, crystallinity, surface area and porosity. In general, the specific surface area and crystallinity can be colliding factors in determination of photocatalytic activity, as a large surface area often results from a porous structure and corresponds to semiconductors with lower crystallinity [66]. This lower crystallinity is attributed to defects present in the crystal structure where it facilitates electron-hole pair recombination, thus reducing the photocatalytic activity.

3.2.5. Degradation kinetics

Fig. 13a and b show the $\ln(COD/COD_0)$ as a function of time and represent a straight line. The slope of linear regression is equal to the first-order apparent rate constant *k*. Their corresponding values for two pH levels (5 and 9) and different initial concentrations are regrouped in Table 3, it can be seen that there is an excellent relationship between the irradiation time and $\ln(COD/COD_0)$, which confirms that the photocatalytic degradation of solvent follows first-order kinetics. The reaction rate varies with the complexity of the degradation, the amount of substrate adsorbed on the catalyst surface, and the absorption spectra of the substrate. When substrates with high UV absorption coefficients are overused, they cover the catalyst surface and prevent radiation penetration [67].

According to Zolfaghari et al. [68], who studied the degradation of the solvent through the TiO_2/UV photocatalytic process, it was found that for efficient decomposition the optimal loading is 0.1% by weight providing sufficient surface area for the reaction, with no irradiation loss occurring due to ultraviolet light scattering. The photocatalytic degradation of organic compounds usually follows first-order kinetics. However, the reaction rate varies with the complexity of the degradation, the amount of substrate adsorbed on the catalyst surface, and the absorption spectra of the substrate. Studies with nanomaterials (nanotubes, nanocylinders, nanoplates, nanospheres and nanoparticles) with tuned structural and textural properties have been evaluated in the photocatalytic degradation process of solvents and subjected to UV [69].

Table 3 lists the first order rate constants (*k*) for the different levels of pH, solvent and loading of the TiO_2 photocatalyst. All experiments showed good linear fits of the pseudo-first-order model.

According to the degradation mechanism, photogenerated electrons (e^-) were excited by visible light irradiation from valence band (VB), which were transported to conduction band (CB) providing holes for VB. They exhibited excellent potency to generate $^{\bullet}OH$ radicals in solvent solution by capturing photogenerated electrons. The $^{\bullet}OH$ radicals were known to be the most important and powerful oxidizing species, which could effectively oxidize various organic compounds into CO_2 and H_2O which creates an oxygen gap that decreases the decomposition rate [70].

In this research, the chain reaction model involves $^{\bullet}OH$ radicals and photogenerated electron-hole pairs in the presence of solvents with TiO_2 producing a large number of hydroxylated products, which are degraded. The main surfactant sites mainly oxidize the solvent molecules by

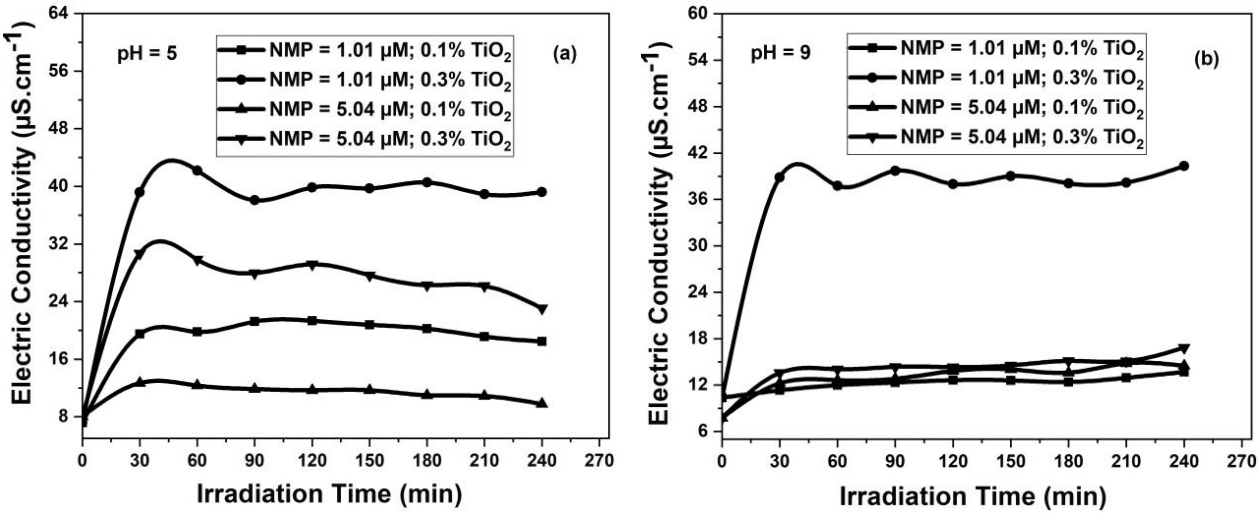

Fig. 12. Conductivity curve for NMP (a) pH 5 and (b) pH 9.

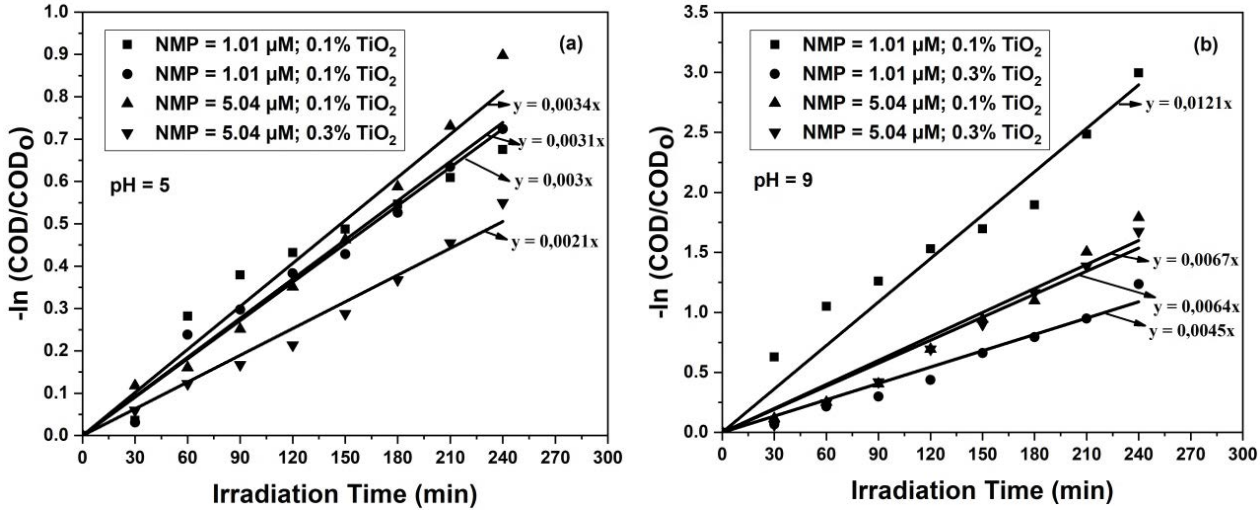

Fig. 13. Linear transformation for the degradation of NMP (a) pH 5 and (b) pH 9.

TiO_2 where they were considered as photogenerated electron holes and •OH radicals. The photogenerated electrons available in the CB can be allocated to the CB from TiO_2 to produce superoxide radicals ($^{\bullet}O_2^-$) after reacting with the oxygen molecules. TiO_2 as a photocatalyst present at the interface between the organic and aqueous phase makes possible the degradation of solvents on the surface of TiO_2 and easily reacts with the •OH radicals produced in the photocatalytic degradation system, resulting in excellent solvent degradation [71].

Analyzing NMP solvent at pH 5 levels resulted in k values of 0.0031, 0.003, 0.0034 and 0.0021 min^{-1}, while for pH 9 k values of 0.0121, 0.0045, 0.0067 and 0.0064 min^{-1} were obtained. However, pH has a very significant effect on the degradation rates, as the degradation rate constant is higher. For the NMP solvent at pH 5, the linear regression values were 0.98, 0.99, 0.99 and 0.99. For pH 9, the linear regression values were 0.98, 0.98, 0.98 and 0.98. This clearly indicates that the photocatalytic degradation reaction obeys first-order kinetics. In alkaline medium, the efficiency is higher than in acidic medium, and the process is more effective when the values of solvent concentration and photocatalyst loading are lower.

3.2.6. Statistical analysis

From Fig. 14 we can observe in (a) the surface curves and in (b) the contour curves, relating the influence of pH and TiO_2 variables with the photocatalytic degradation response of NMP, respectively.

According to Fig. 14 it was possible to observe that the darker regions indicate the best conditions for the factors related to the COD removal efficiency. From the images, it is quite evident that the pH variable had a positive effect on the degradation response variable, showing that, with decrease photocatalyst loading and increasing pH, a better

Table 3
Kinetic parameters in NMP degradation after the photocatalytic reaction

Exp.	Solvent concentration (μM)	Catalyst charge (%)	pH	COD_0	COD_f	η (%)	k (min^{-1})	$t_{½}$ (min)	R^2
1	1.01	0.10	5	2,987.42	1,519.92	49.12	0.0031	223.59	0.98
2	1.01	0.30	5	3,402.06	1,649.48	51.52	0.0030	231.05	0.99
3	5.04	0.10	5	1,418.06	577.73	59.26	0.0034	203.87	0.99
4	5.04	0.30	5	2,634.24	1,519.76	42.31	0.0021	330.07	0.99
5	1.01	0.10	9	3,061.22	153.06	95.00	0.0121	57.28	0.98
6	1.01	0.30	9	1,512.19	439.02	70.97	0.0045	154.03	0.98
7	5.04	0.10	9	915.56	152.59	83.33	0.0067	103.45	0.98
8	5.04	0.30	9	1,729.73	324.32	81.25	0.0064	108.30	0.98

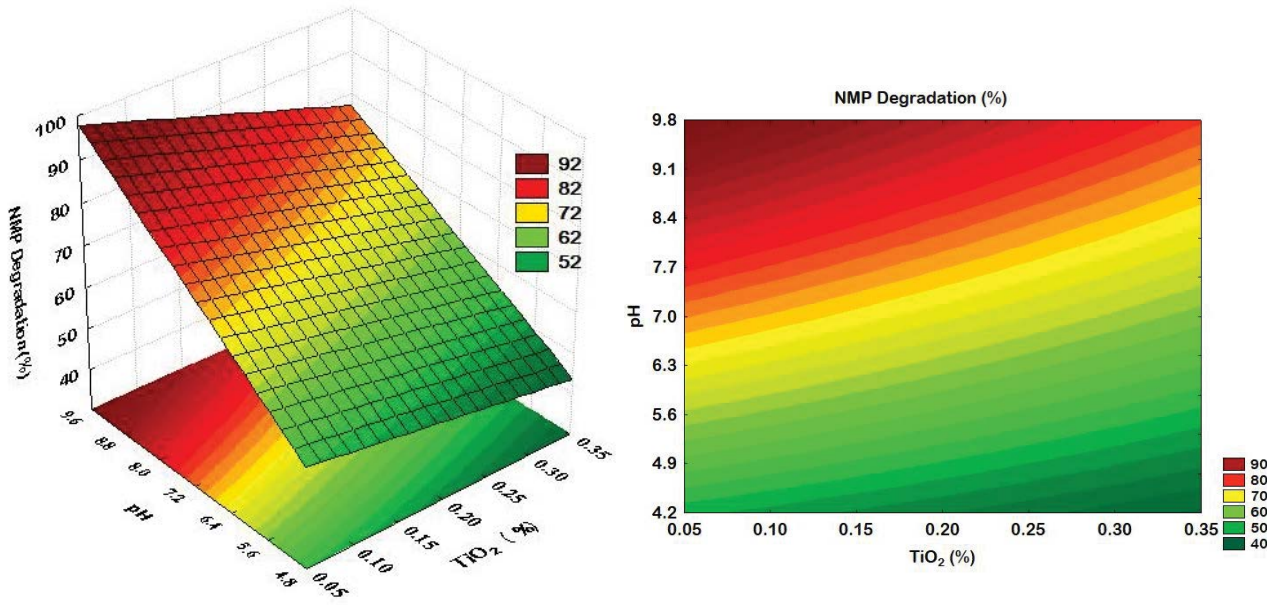

Fig. 14. Representation of pH behavior for NMP (a) surface and (b) contour.

photocatalytic degradation is obtained. This fact occurred because the main surfactant sites mainly oxidize the NMP solvent molecules by TiO_2, where they were considered as photogenerated electron holes and •OH radicals. For the photocatalytic degradation response, the pH variable indicates that the solvent reduction in the effluent is proportional to the level of this variable. TiO_2 increases the number of active sites in the medium and, consequently, causes a greater reduction in the amount of NMP concentration. Furthermore, it was observed that the degradation was favored in alkaline medium, since higher degradation values were observed at pH 9. Analyzing the influence of pH, the adjustment with sodium hydroxide increased the degradation capacity at the two pHs evaluated. The highest percentages were obtained at pH 9, reaching 95% reduction of MPN.

By means of the statistical technique for experimental data involving quantitative measurements, the analysis of variance (ANOVA) where the regression significance and lack of fit at the 95% confidence level ($p < 0.05$) for photocatalytic degradation is checked, using the F test, as shown in Table 4. It can be seen from Table 4 that the model showed significant regression at the 95% confidence level (F significance), showing that the models resulted in values greater than 95% of the variance of the experimental data for reducing photocatalytic degradation of NMP solvent.

3.2.7. Pollutant degradation

Fig. 15 shows the total degradation percentages of the pollutant NMP. Analyzing the results obtained in the experiments, the best response obtained had a photocatalytic degradation of 95%. Table 5 illustrates the experimental levels and their respective variables for NMP degradation.

The photocatalytic activity of the visualized samples was evaluated through the degradation of the solvent NMP and these values were estimated through preliminary tests.

From Fig. 15 it is seen that the organic matter removal efficiency improved even more when the catalyst loading was reduced from 0.3% to 0.1%, with the pH at 9 and the solvent concentration at 1.01 μM NMP combined with

Table 4
Analysis of variance (ANOVA) of 8 experiments conducted for NMP

Exp.	Variations causes	Degree of freedom (DF)	Sum of squares (SS)	Mean squares (MS)	Value of $F_{calculated}$	F significance[a]
1	Regression	1	50,716.62	50,716.62	108.12	1.65E^{-05}
	Residue	7	3,283.38	469.05		
	Total	8	54,000.00			
2	Regression	1	53,038.06	53,038.06	385.95	2.21E^{-07}
	Residue	7	961.94	137.42		
	Total	8	54,000.00			
3	Regression	1	52,915.80	52,915.80	341.64	3.36E^{-07}
	Residue	7	1,084.19	154.88		
	Total	8	54,000.00			
4	Regression	1	53,174.83	53,174.83	451.08	1.29E^{-07}
	Residue	7	825.17	117.88		
	Total	8	54,000.00			
5	Regression	1	52,243.45	52,243.45	208.19	1.83E^{-06}
	Residue	7	1,756.55	250.93		
	Total	8	54,000.00			
6	Regression	1	52,753.37	52,753.37	296.22	5.49E^{-07}
	Residue	7	1,246.63	178.09		
	Total	8	54,000.00			
7	Regression	1	52,603.23	52,603.23	263.62	8.18E^{-07}
	Residue	7	1,396.77	199.54		
	Total	8	54,000.00			
8	Regression	1	53,253.78	53,253.78	499.55	9.08E^{-08}
	Residue	7	746.22	106.60		
	Total	8	54,000.00			

[a]Statistically significant with α = 5% probability.

Table 5
Experimental planning matrix for TiO_2 photocatalysis

Experiments	Variables			%Degradation
	TiO_2	NMP	pH	
1	–	–	–	49
2	+	–	–	51
3	–	+	–	59
4	+	+	–	42
5	–	–	+	95
6	+	–	+	70
7	–	+	+	83
8	+	+	+	81

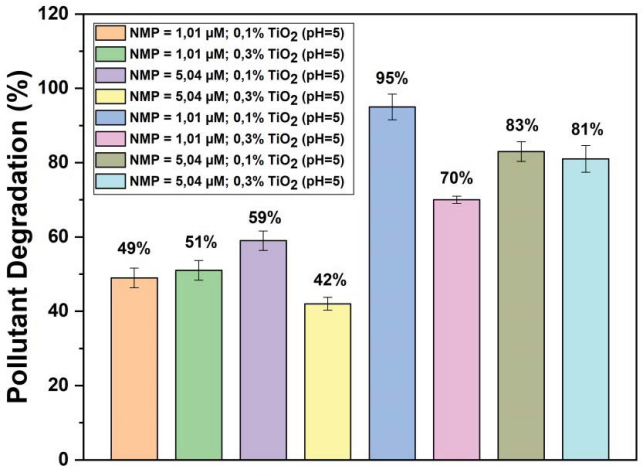

Fig. 15. NMP solvent degradation

ultraviolet radiation, as shown in Table 5. Thus, there is a removal efficiency around 95%, a value considered very interesting due to the complexity of treating the organic matter present in effluent generated in the membrane production by the phase inversion technique.

4. Conclusion

The study of COD analysis was observed through the reaction kinetics of AOP with TiO_2/UV, where its decay during photocatalytic degradation was fitted to the first order kinetic model. From the Statistic tool it was detected that the pH was the most significant operational parameter, and its relationship was directly proportional to the degradation of contaminants. The highest NMP removal efficiency of 95% was obtained at pH 9 with the lowest solvent concentration and lowest catalyst percentage of 0.1%.

TiO_2/UV heterogeneous photocatalysis can be used and considered as a promising process for the photodegradation of NMP solvent, because independent of the concentration of organics and at pH 9 it was found a removal efficiency ranging from 70%–95% of the contaminants present in effluents generated in obtaining hybrid membranes produced by phase inversion technique.

Acknowledgment

The present work was carried out with the assistance of the DESA/UEPB and UAEMa/UFCG laboratories. The authors would like to thank CNPq and CAPES for their scholarships and financial support.

References

[1] Z. Pan, C. Song, L. Li, H. Wang, Y. Pan, Y. Wang, X. Feng, Membrane technology coupled with electrochemical advanced oxidation processes for organic wastewater treatment: recent advances and future prospects, Chem. Eng. J., 376 (2019) 120909, doi: 10.1016/j.cej.2019.01.188.
[2] M.A. Rauf, M.A. Meetani, A. Khaleel, A. Ahmed. Photocatalytic degradation of methylene blue using a mixed catalyst and product analysis by LC/MS, Chem. Eng. J., 157 (2010) 373–378.
[3] E.D.S. Nascimento, A. Tenuta Filho, Chemical waste risk reduction and environmental impact generated by laboratory activities in research and teaching institutions, Braz. J. Pharm. Sci., 46 (2010) 187–198.
[4] D. Zhang, F. Zeng, Visible light-activated cadmium-doped ZnO nanostructured photocatalyst for the treatment of methylene blue dye, J. Mater. Sci., 47 (2012) 2155–2161.
[5] N.B. Swan, M.A.A. Zaini, Adsorption of malachite green and congo red dyes from water: recent progress and future outlook, Ecol. Chem. Eng. S, 26 (2019) 119–132.
[6] F.J. Lozano, R. Lozano, P. Freire, C.J. Gonzalez, T. Sakao, M.G. Ortiz, A. Trianni, A. Carpenter, T. Viveros, New perspectives for green and sustainable chemistry and engineering: approaches from sustainable resource and energy use, management, and transformation, J. Cleaner Prod., 172 (2018) 227–232.
[7] R. Monsef, M.G. Arani, M.S. Niasari, Design of magnetically recyclable ternary Fe_2O_3/$EuVO_4$/g-C_3N_4 nanocomposites for photocatalytic and electrochemical hydrogen storage, ACS Appl. Energy Mater., 4 (2021) 680–695.
[8] S.Z. Ajabshir, M.S. Morassaei, M.S. Niasari, Eco-friendly synthesis of $Nd_2Sn_2O_7$ – based nanostructure materials using grape juice as green fuel as photocatalyst for the degradation of erythrosine, Composites, Part B, 167 (2019) 643–653.
[9] S.A.F. Fini, M.S. Niasari, D. Ghanbari, Hydrothermal green synthesis of magnetic Fe_3O_4-carbon dots by lemon and grape fruit extracts and as a photoluminescence sensor for detecting of *E. coli* bacteria, Spectrochim. Acta, Part A, 203 (2018) 481–493.
[10] M.S. Niasari, F. Davar, M.R.L. Estarki, Long chain polymer assisted synthesis of flower-like cadmium sulfide nanorods via hydrothermal process, J. Alloys Compd., 481 (2009) 776–780.
[11] S.M.H. Mashkani, F. Mohandes, M.S. Niasari, K.V. Rao, Microwave-assisted synthesis and photovoltaic measurements of $CuInS_2$ nanoparticles prepared by using metal-organic precursors, Mater. Res. Bull., 47 (2012) 3148–3159.
[12] M.S. Niasari, Nanodimensional microreactor-encapsulation of 18-membered decaaza macrocycle copper (II) complexes, Chem. Lett., 34 (2005) 244–245.
[13] M.S. Niasari, Nanoscale microreactor-encapsulation 14-membered nickel (II) hexamethyl tetraaza: synthesis, characterization and catalytic activity, J. Mol. Catal. A: Chem., 229 (2005) 159–164.
[14] R. Monsef, M.G. Arani, O. Amiri, M.S. Niasari, Sonochemical synthesis, characterization and application of $PrVO_4$ nanostructures as an effective photocatalyst for discoloration of organic dye contaminants in wastewater, Ultrason. Sonochem., 61 (2020) 104822, doi: 10.1016/j.ultsonch.2019.104822.
[15] M.S. Niasari, N. Mir, F. Davar, Synthesis and characterization of NiO nanoclusters via thermal decomposition, Polyhedron, 28 (2009) 1111–1114.
[16] M.S. Niasari, F. Davar, Z. Fereshteh, Synthesis of nickel and nickel oxide nanoparticles via heat-treatment of simple octanoate precursor, J. Alloys Compd., 494 (2010) 410–414.
[17] M. Ghanbari, M.S. Niasari, Tl4CdI_6 nanostructures: facile sonochemical synthesis and photocatalytic activity for removal of organic dyes, Inorg. Chem., 57 (2018) 11443–11455.
[18] S. Waclawek, V.V.T. Padil, M. Černík, Major advances and challenges in heterogeneous catalysis for environmental applications: a review, Ecol. Chem. Eng. S, 25 (2018) 9–34.
[19] U.I. Gaya, A.H. Abdullah, M.Z. Hussein, Z. Zainal, Photocatalytic removal of 2,4,6-trichlorophenol from water exploiting commercial ZnO powder, Desalination, 263 (2010) 176–182.
[20] M.M. Arimi, Modified natural zeolite as heterogeneous Fenton catalyst in treatment of recalcitrants in industrial effluent, Prog. Nat. Sci.: Mater. Int., 27 (2017) 275–282.
[21] I.C. M'bra, P. García-Muñoz, P. Drogui, N. Keller, A. Trokourey, D. Robert, Heterogeneous photodegradation of Pyrimethanil and its commercial formulation with TiO_2 immobilized on SiC foams, J. Photochem. Photobiol., A, 368 (2019) 1–6.
[22] M. Afsharnia, M. Kianmehr, H. Biglari, A. Dargahi, A. Karimi, Disinfection of dairy wastewater effluent through solar photocatalysis processes, Water Sci. Eng., 11 (2018) 214–219.
[23] F. Riboni, M.V. Dozzi, M.C. Paganini, E. Giamello, E. Selli, Photocatalytic activity of TiO_2-WO_3 mixed oxides in formic acid oxidation, Catal. Today, 287 (2017) 176–181.
[24] E. Mena, A. Rey, F.J. Beltrán, TiO_2 photocatalytic oxidation of a mixture of emerging contaminants: a kinetic study independent of radiation absorption based on the direct-indirect model, Chem. Eng. J., 339 (2018) 369–380.
[25] S. Ghosh, Visible-Light-Active Photocatalysis: Nanostructured Catalyst Design, Mechanisms, and Applications, 1st ed., Wiley-VCH, Germany, 2018.
[26] S. Waclawek, Do we still need a laboratory to study advanced oxidation processes? a review of the modelling of radical reactions used for water treatment, Ecol. Chem. Eng. S, 28 (2021) 11–28.
[27] R. Baker, Membrane Technology and Applications, 2nd ed., John Wiley & Sons Inc., California, 2004.
[28] M. Mulder, Basic Principles of Membrane Technology, 2nd ed., Springer, Netherlands, 1996.
[29] C.H. Loh, B. Wu, L. Ge, C. Pan, R.Wang, High-strength N-methyl-2-pyrrolidone-containing process wastewater treatment using sequencing batch reactor and membrane bioreactor: a feasibility study, Chemosphere, 194 (2018) 534–542.
[30] M. Razali, J.F. Kim, M. Attfield, P.M. Budd, E. Drioli, Y.M. Lee, G. Szekely, Sustainable wastewater treatment and recycling in membrane manufacturing, Green Chem., 17 (2015) 5196–5205.
[31] R.B. Baird, Standard Methods for the Examination of Water and Wastewater, 23rd ed., Water Environment Federation, American Public Health Association, 2017.
[32] C.A.P. Lima, B.A. Araujo, K.S. Silva, C.B. Silva, G.G.C. Lima, F.F. Vieira, K.M. Medeiros, Advanced oxidative process by heterogeneous photocatalysis for chemical laboratories effluents treatment, Desal. Water Treat., 174 (2020) 248–257.
[33] K.M. Reza, A.S.W. Kurny, F. Gulshan, Parameters affecting the photocatalytic degradation of dyes using TiO_2: a review, Appl. Water Sci., 7 (2017) 1569–1578.
[34] S. Papoutsakis, S. Miralles-Cuevas, N. Gondrexon, S. Baup, S. Malato, C. Pulgarin, Coupling between high-frequency ultrasound and solar photo-Fenton at pilot scale for the treatment of organic contaminants: an initial approach, Ultrason. Sonochem., 22 (2015) 527–534.
[35] A. Peter, A. Mihaly-Cozmuta, C. Nicula, L. Mihaly-Cozmuta, A. Jastrzębska, A. Olszyna, L. Baia, UV light-assisted degradation of methyl orange, methylene blue, phenol, salicylic

acid, and rhodamine B: photolysis versus photocatalyis, Water Air Soil Pollut., 228 (2017) 1–12.
[36] T. Soltani, M.H. Entezari, Photolysis and photocatalysis of methylene blue by ferrite bismuth nanoparticles under sunlight irradiation, J. Mol. Catal. A: Chem., 377 (2013) 197–203.
[37] M. Sanchez, M.J. Rivero, I. Ortiz, Kinetics of dodecylbenzenesulphonate mineralisation by TiO_2 photocatalysis, Appl. Catal., B, 101 (2011) 515–521.
[38] F. Kazemi, Z. Mohamadnia, B. Kaboudin, Z. Karimi, Photodegradation of methylene blue with a titanium dioxide/polyacrylamide photocatalyst under sunlight, J. Appl. Polym. Sci., 133 (2016) 43386, doi: 10.1002/app.43386.
[39] T. Soltani, M.H. Entezari, Photolysis and photocatalysis of methylene blue by ferrite bismuth nanoparticles under sunlight irradiation, J. Mol. Catal. A: Chem., 377 (2013) 197–203.
[40] R. Ameta, S.C. Ameta, Photocatalysis: Principles and Applications, 1st ed., CRC Press Taylor & Francis Group, Boca Raton, 2017.
[41] H. Zangeneh, A.A.L. Zinatizadeh, M. Habibi, M. Akia, M.H. Isa, Photocatalytic oxidation of organic dyes and pollutants in wastewater using different modified titanium dioxides: a comparative review, J. Ind. Eng. Chem., 26 (2015) 1–36.
[42] A. Matioli, J. Miagava, D. Gouvêa, Modification of the stability of nanometric TiO_2 polymorphs by excess SnO_2 surface, Ceramics, 58 (2012) 53–57.
[43] J. Dostanic, B. Grbic, N. Radic, S. Stojadinovic, R. Vasilic, Z. Vukovic, Preparation and photocatalyic properties of TiO_2-P25 film prepared by spray pyrolysis method, Appl. Surf. Sci., 274 (2013) 321–327.
[44] Z. Zarhri, M.A.A. Cardos, Y. Ziat, M. Hammi, O.E. Rhazouani, J.C.C. Argüello, D.A. Avellaneda, Synthesis, structural and crystal size effect on the optical properties of sprayed TiO_2 thin films: experiment and DFT TB-mbj, J. Alloys Compd., 819 (2020) 153010, doi: 10.1016/j.jallcom.2019.153010
[45] Y. Zhang, Z.Z. Fang, P. Sun, Z. Huang, S. Zheng, A study on the synthesis of coarse TiO_2 powder with controlled particle sizes and morphology via hydrolysis, Powder Technol., 393 (2021) 650–658.
[46] J. Dostanić, B. Grbić, N. Radić, S. Stojadinović, R. Vasilić, Z. Vuković, Preparation and photocatalyic properties of TiO_2-P25 film prepared by spray pyrolysis method, Appl. Surf. Sci., 274 (2013) 321–327.
[47] S. Sohrabnezhad, Study of catalytic reduction and photodegradation of methylene blue by heterogeneous catalyst, Spectrochim. Acta, Part A, 81 (2011) 228–235.
[48] E.L. Castellanos-Leala, P. Acevedo-Peñab, V.R. Güiza-Argüelloc, E.M. Córdoba-Tutaa, N and F co-doped TiO_2 thin films on stainless steel for photoelectrocatalytic removal of cyanide ions in aqueous solutions, Mater. Res., 20 (2017) 487–495.
[49] B. Choudhury, A. Choudhury, Luminescence characteristics of cobalt doped TiO_2 nanoparticles, J. Lumin., 132 (2012) 178–184.
[50] L.G. Devi, B.N. Murhty, S.G. Kumar, Photocatalytic degradation of imidachloprid under solar light using metal ion doped TiO_2 nanoparticles: influence of oxidation state and electronic configuration of dopants, Catal. Lett., 130 (2009) 496–503.
[51] P. Ngaotrakanwiwat, P. Heawphet, P. Rangsunvigit, Enhancement of photoelectrochemical cathodic protection of copper in marine condition by Cu-doped TiO_2, Catalysts, 10 (2020) 146–155.
[52] X. Yang, Y. Wang, L. Zhang, H. Fu, P. He, D. Han, T. Lawson, X. An, The use of tunable optical absorption plasmonic Au and Ag decorated TiO_2 structures as efficient visible light photocatalysts, Catalysts, 10 (2020) 139–153.
[53] S. Joseph, B. Mathew, Microwave assisted biosynthesis of silver nanoparticles using the rhizome extract of alpinia galanga and evaluation of their catalytic and antimicrobial activities, J. Nanopart., 2014 (2014) 1–9.
[54] K. Dai, H. Chen, T. Peng, D. Ke, H. Yi, Photocatalytic degradation of methyl orange in aqueous suspension of mesoporous titania nanoparticles, Chemosphere, 69 (2007) 1361–1367.
[55] C. Marinescu, A. Sofronia, C. Rusti, R. Piticescu, V. Badilita, E. Vasile, R. Baies, S. Tanasescu, DSC investigation of nanocrystalline TiO_2 powder, J. Therm. Anal. Calorim., 103 (2011) 49–57.
[56] S.D. Delekar, H.M. Yadav, S.N. Achary, S.S. Meena, S.H. Pawar, Structural refinement and photocatalytic activity of Fe-doped anatase TiO_2 nanoparticles, Appl. Surf. Sci., 263 (2012) 536–545.
[57] J.C. Yu, J. Yu, W. Ho, Z. Jiang, L. Zhang, Effects of F^- Doping on the photocatalytic activity and microstructures of nanocrystalline TiO_2 powders, Chem. Mater., 14 (2002) 3808–3816.
[58] V.G. Gandhi, M.K Mishra, M.S. Rao, A. Kumar, P.A. Joshi, D.O. Shah, Comparative study on nano-crystalline titanium dioxide catalyzed photocatalytic degradation of aromatic carboxylic acids in aqueous medium, J. Ind. Eng. Chem., 17 (2011) 331–339.
[59] S.J. Darzi, A.R. Mahjoub, A. Nilchi, Synthesis of spongelike mesoporous anatase and its photocatalytic properties, J. Chem. Chem. Eng., 29 (2010) 37–42.
[60] J. Liu, Q. Zhang, J. Yang, H. Ma, M.O. Tade, S. Wang, J. Liu, Facile synthesis of carbon-doped mesoporous anatase TiO_2 for the enhanced visible-light driven photocatalysis, Chem. Commun., 50 (2014) 13971–13974.
[61] C. Yogi, K. Kojima, N. Wada, H. Tokumoto, T. Takai, T. Mizoguchi, H. Tamiaki, Photocatalytic degradation of methylene blue by TiO_2 film and Au particles-TiO_2 composite film, Thin Solid Films, 516 (2008) 5881–5884.
[62] R.S. Dariani, A. Esmaeili, A. Mortezaali, S. Dehghanpour, Photocatalytic reaction and degradation of methylene blue on TiO_2 nano-sized particles, Optik, 127 (2016) 7143–7154.
[63] A.H. Jawad, N.S.A. Mubarak, M.A.M. Ishak, K. Ismail, W.I. Nawawi, Kinetics of photocatalytic decolourization of cationic dye using porous TiO_2 film, J. Taibah Univ. Sci., 10 (2016) 352–362.
[64] C.M. Marrodan, F. Liguori, P. Barbaro, Sustainable processes for the catalytic synthesis of safer chemical substitutes of N-methyl-2-pyrrolidone, Mol. Catal., 466 (2019) 60–69.
[65] N. Mandzy, E. Grulke, T. Druffel, Breakage of TiO_2 agglomerates in electrostatically stabilized aqueous dispersions, Powder Technol., 160 (2005) 121–126.
[66] Z. He, Z. Zhu, J. Li, J. Zhou, N. Wei, Characterization and activity of mesoporous titanium dioxide beads with high surface areas and controllable pore sizes, J. Hazard. Mater., 190 (2011) 133–139.
[67] J.P.S. Valente, P.M. Padilha, A.O. Florentino, Studies on the adsorption and kinetics of photodegradation of a model compound for heterogeneous photocatalysis onto TiO_2, Chemosphere, 64 (2006) 1128–1133.
[68] A. Zolfaghari, H.R. Mortaheb, F. Meshkini, Removal of N-methyl-2-pyrrolidone by photocatalytic degradation in a batch reactor, Ind. Eng. Chem. Res., 50 (2011) 9569–9576.
[69] S.D.A. Pascoal, C.B. Silva, K.S. Silva, G.G.C. Lima, K.M. Medeiros, C.A.P. Lima, Treatment by TiO_2/UV of wastewater generated in polymeric membranes production, Desal. Water Treat., 207 (2020) 30–42.
[70] K.J. Parton, B.J. Godley, D. Santillo, M. Tausif, L.C.M. Omeyer, T.S. Galloway, Investigating the presence of microplastics in demersal sharks of the North-East Atlantic, Sci. Rep., 10 (2020) 1–11.
[71] X. Wang, L. Cao, D. Chen, R.A. Caruso, Engineering of monodisperse mesoporous titania beads for photocatalytic applications, ACS Appl. Mater. Interfaces, 5 (2013) 9421–9428.